

Small Signal Analysis of SQUID Direct Readout Schemes

Yongliang Wang^{a,b,c,*}, Guofeng Zhang^{a,b}, Shulin Zhang^{a,b},

Liangliang Rong^{a,b}, Yong Wang^c, Xiaoming Xie^{a,b}

^a *State Key Laboratory of Functional Materials for Informatics, Shanghai Institute of Microsystem and Information Technology (SIMIT), Chinese Academy of Sciences (CAS), Shanghai 200050, China*

^b *Chinese Academy of Science, Center for Excellence in Superconducting Electronics, Shanghai 200050, China*

^c *Department of Automation, University of Science and Technology of China, Hefei 230027, China*

*Corresponding author. Tel.: +86 02162511070; Fax: +86 02162127493.

E-mail address: wangyl@mail.sim.ac.cn

Abstract

To better understand working principles of Superconducting Quantum Interference Device (SQUID) direct readout schemes which are working in different bias and amplifier modes with different internal feedback schemes, we present the complete circuit analyses based on SQUID small signal model. SQUID bias and amplifier circuits are analyzed using SQUID Thevenin's equivalent circuit, and the general equivalent circuit of SQUID with different internal feedback schemes is derived and analyzed with trans-impedance amplifier model. Transfer characteristics and noise performances of different direct readout schemes are analyzed and experimentally characterized. It is shown that, amplifier noise suppression is only depended on SQUID flux-to-voltage transfer coefficient and irrelevant to the configuration of bias and amplifier; SQUID with internal feedback scheme improves the transfer coefficient with voltage feedback, and regulates the dynamic resistance with current feedback.

Keywords: SQUID, direct readout, voltage feedback, current feedback.

1. Introduction

Direct Current Superconducting Quantum Interference Device (DC SQUID) is sensitive non-linear flux-to-voltage convertor [1], which has to be used in the Flux-Locked Loop (FLL) to realize linear flux measurement [2]. Typical FLL consists of SQUID, amplifier, integrator and flux feedback circuit as shown in Fig. 1. Readout circuit is referred as SQUID and its amplifier in this paper. Room temperature amplifier is directly coupled with SQUID without Flux Modulation (FM) scheme [3] in the direct readout schemes, which were developed rapidly to build simple and compact readout electronics for practical multichannel SQUID systems, e.g., Magneto-Cardiogram (MCG). The challenge of direct readout FLL is the noise mismatching between SQUID and amplifier which voltage noise is usually ten times of SQUID intrinsic noise and dominates the noise performance of FLL.

Several internal feedback circuits around SQUID were introduced to suppress amplifier noise. Additional Positive Feedback (APF) was firstly presented by D.Drung *et al.* in early 1990s [4-6], and the same scheme working under voltage bias was called Noise Cancellation (NC) [7, 8]. Furthermore, Bias Current Feedback (BCF) circuit was introduced to suppress external current noise in addition to APF [9, 10], meanwhile, the SQUID Bootstrap Circuit (SBC) evolved from APF and BCF was also developed for working under voltage bias [11, 12]. Overall behaviors and working principles of those readout schemes were usually analyzed by considering SQUID and amplifier separately [13], and studied individually [14, 15]. However, those various readout concepts are confusing users in their readout electronics design. The more common circuit analyses of SQUID direct readout schemes are required.

In this paper, we will present complete circuit analyses of SQUID direct readout schemes based on the small signal circuit model in form of Thevenin's equivalent circuit. We will firstly present two general configurations of bias and amplifier, and bring out the general equivalent circuit of all the SQUID internal feedback schemes, and then analysis the transfer coefficient and noise performance of low noise direct readout schemes which are the combinations of different bias modes and internal feedback schemes. Finally, the experimental results are presented and discussed.

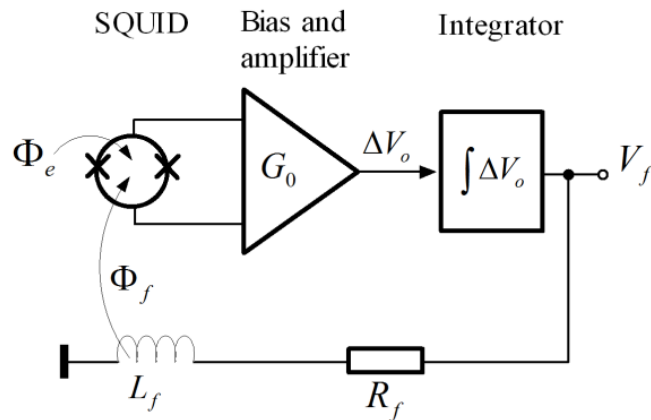


Fig. 1. Equivalent circuit of direct readout FLL.

2. SQUID bias and amplifier circuit

2.1 Two SQUID bias and amplifier circuits

SQUID is directly coupled with the bias and amplifier circuit in the direct readout FLL as shown in Fig.1. There are only two common configurations of bias and amplifier circuit in the existing SQUID direct readout schemes [2, 16]. The one shown in Fig. 2a is called Current-Bias-Voltage-Amplifier (CBVA) mode, the other shown in Fig. 2c is called Voltage-Bias-Current-Amplifier (VBCA) mode. The details are in the following:

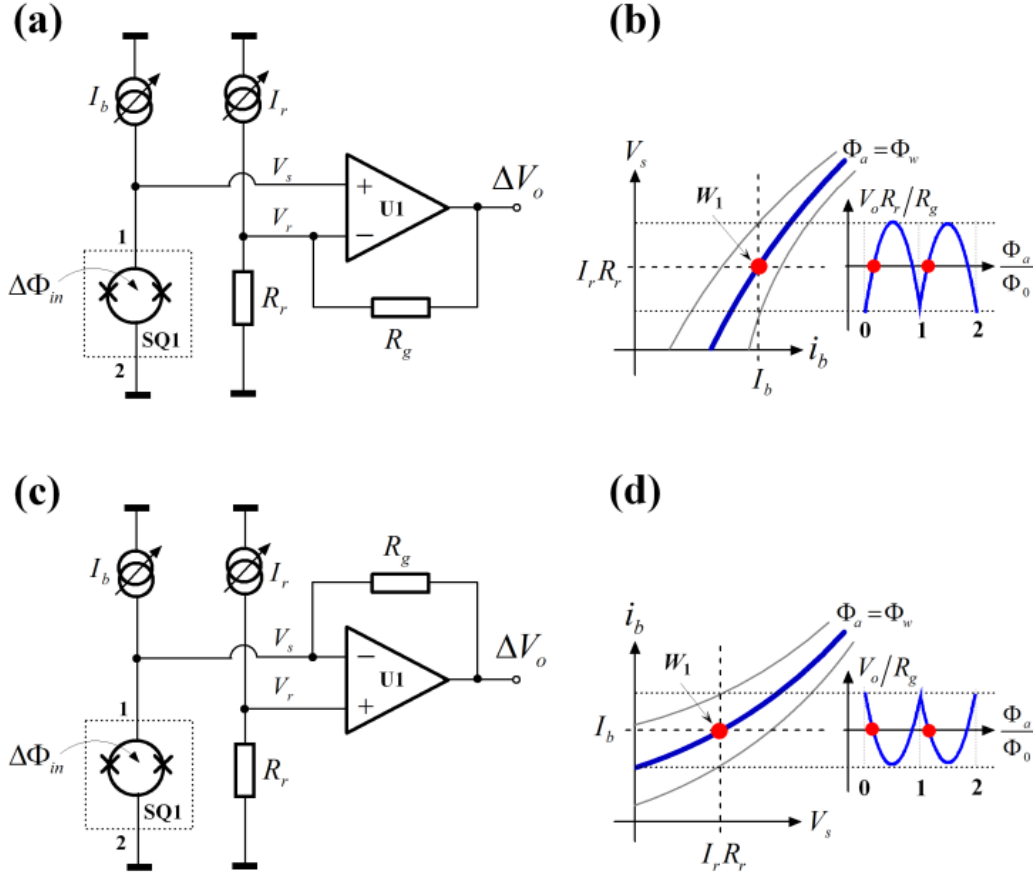


Fig. 2. (a) SQUID direct readout circuit with CBVA, (b) Illustration of flux-to-voltage characteristics read out with CBVA, (c) SQUID direct readout circuit with VBCA, (d) Illustration of flux-to-current characteristics read out with VBCA.

1) Bias circuit is an H-type bridge, in which two-terminal SQUID SQ1 and reference resistor R_r are two compatible arms. Both are biased with current I_b and I_r respectively, where, V_s is voltage output of SQ1, and V_r is voltage of reference resistor R_r . V_s can be described with a function of bias current i_b and applied flux Φ_a , i.e., $V_s = f(i_b, \Phi_a)$, according to its bias-dependant flux-to-voltage transfer characteristics.

2) Differential amplifier is implemented using a low noise operational amplifier in closed-loop with feedback resistor R_g connected at its non-inverting input and voltage output as shown in Fig. 2a and c. In practical, $R_g \gg R_r$, the current shunted by R_g is neglected in the following analyses.

3) In CBVA mode, V_s is connected to the non-inverting input, and V_r is connected to the inverting input of amplifier, where, SQ1 is biased under current I_b , and R_r is driven by current from I_r and V_o , thus, $V_s = f(I_b, \Phi_a)$, $V_r = R_r(I_r + V_o / R_g)$.

4) In VBCA mode, the connection is reversed, where, SQ1 was driven by current from I_b and V_o , and R_r is biased by I_r , thus, $V_s = f((I_b + V_o / R_g), \Phi_a)$, $V_r = R_r I_r$.

Since, differential inputs of closed-loop operational amplifier are “shorted” [17], i.e., $V_s = V_r$. The Φ_a -to- V_o characteristics read out with CBVA exhibit the flux-to-voltage characteristics of SQ1 as illustrated in Fig. 2b. The Φ_a -to- V_o characteristics read out with VBCA exhibit the flux-to-current characteristics of SQ1 as illustrated in Fig. 2d. Characteristics of SQUID read out with CBVA and VBCA are totally different [11].

However, when FLL is working in closed-loop with null input of integrator [2], i.e., $V_o=0$, working point of SQ1 in both amplifier modes is same as defined in (1), where, current of SQ1 is I_b , and voltage output is $I_r R_r$; Φ_w is the background flux on the working point in the absence of external flux.

$$f(I_b, \Phi_w) = I_r R_r \quad (1)$$

2.2 Small signal analysis of amplifier circuits

Around the working point, small signal model of SQ1 is extracted from its total differential of SQUID flux-to-voltage function as:

$$\begin{aligned} \Delta V_s &= f(I_b + \Delta I_b, \Phi_w + \Delta \Phi_a) - f(I_b, \Phi_w) \\ &\cong \frac{\partial V_s}{\partial \Phi_a} \Delta \Phi_a + R_d \Delta I_b \end{aligned} \quad (2)$$

Where, $\partial V_s / \partial \Phi_a$ is the flux-to-voltage transfer coefficient, and R_d is the dynamic resistance, they are defined as:

$$\begin{cases} \frac{\partial V_s}{\partial \Phi_a} = \left. \frac{\partial f}{\partial \Phi_a} \right|_{i_b=I_b, \Phi_a=\Phi_w} \\ R_d = \left. \frac{\partial f}{\partial i_b} \right|_{i_b=I_b, \Phi_a=\Phi_w} \end{cases} \quad (3)$$

SQUID small signal model is implemented in form of the Thevenin’s equivalent circuit [18], which is a flux-driven voltage source in series with an internal resistor as shown in Fig. 3a and b. $(\partial V_s / \partial \Phi_a) \Delta \Phi_a$ is thus the flux-driven voltage, and R_d is the internal resistance.

SQUID working with CBVA and VBCA implement small signal flux-to-voltage conversion before integrator with $\Delta \Phi_{in}$ as flux input and ΔV_o as voltage output. $\Delta V_o / \Delta \Phi_{in}$ is thus the overall flux-to-voltage transfer coefficient of direct readout circuit, and is part of the open-loop gain of FLL.

The equivalent small signal readout circuits are shown in Fig. 3a and b, where, $\Delta \Phi_{in}$ comes from external input flux Φ_e and feedback flux Φ_f as shown in Fig. 1. Since, $\Delta \Phi_a = \Delta \Phi_{in}$, the small signal voltage of SQ1 is $(\partial V_s / \partial \Phi_a) \Delta \Phi_{in}$. SQ1 with CBVA is known as non-inverting amplifier circuit with gain of R_g / R_r [17]. Its $\Delta \Phi_{in}$ -to- ΔV_o

transfer coefficient is derived as:

$$\left(\frac{\Delta V_o}{\Delta \Phi_{in}}\right)_{CBVA} = \frac{R_g}{R_r} \frac{\partial V_s}{\partial \Phi_a} \quad (4)$$

Meanwhile, SQ1 with VBCA is known as inverting amplifier circuit with gain of $-R_g/R_d$ [17]. Its $\Delta \Phi_{in}$ -to- ΔV_o transfer coefficient is written as:

$$\left(\frac{\Delta V_o}{\Delta \Phi_{in}}\right)_{VBCA} = -\frac{R_g}{R_d} \frac{\partial V_s}{\partial \Phi_a} \quad (5)$$

If $R_r = R_d$, the overall transfer coefficients in (4) and (5) are equivalent with opposite sign. However, $\partial V_s/\partial \Phi_a$ can be directly characterized in CBVA mode, but not in VBCA mode.

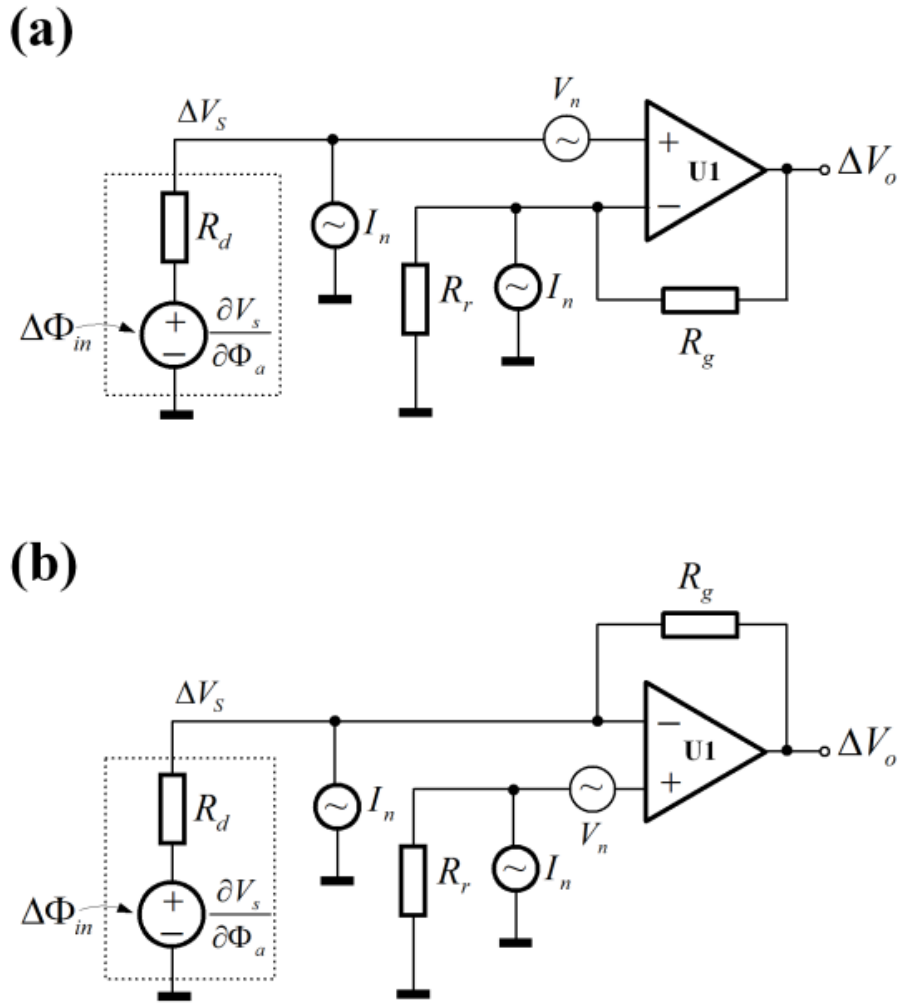


Fig. 3. (a) Small signal circuit of SQUID working with CBVA, (b) Small signal circuit of SQUID working with VBCA.

Equivalent flux noise of amplifier Φ_n is the another key parameter which determines the noise performance of FLL. By introducing voltage noise V_n and current noise I_n of operational amplifier to the equivalent small signal readout circuits, the total noise contributions in both VBCA and CBVA circuits are the Root Mean

Square (RMS) of V_n and voltage noises generated by I_n on R_d and R_r . Φ_n is derived as:

$$\Phi_n = \frac{\sqrt{V_n^2 + (I_n R_d)^2 + (I_n R_r)^2}}{\partial V_s / \partial \Phi_a} \cong \frac{V_n}{\partial V_s / \partial \Phi_a} \quad (6)$$

Voltage noise V_n is the dominant noise, and current noise I_n can be neglected if R_d and R_r meet the noise impedance matching condition as expressed in (7), where, R_n is defined as the noise impedance of amplifier U1.

$$R_d < R_n; R_r < R_n; R_n = \frac{V_n}{I_n} \quad (7)$$

It is shown that equivalent flux noise of amplifier is irrelevant to amplifier configurations [13, 19], and is only determined by $\partial V_s / \partial \Phi_a$ of SQUID as noise impedance matching condition is satisfied.

3. SQUID with internal feedback circuit

3.1 SQUID internal feedback schemes

SQUID with internal feedback circuits are developed to improve transfer coefficient for amplifier noise suppression. There are three typical internal feedback schemes as shown in Fig. 4.

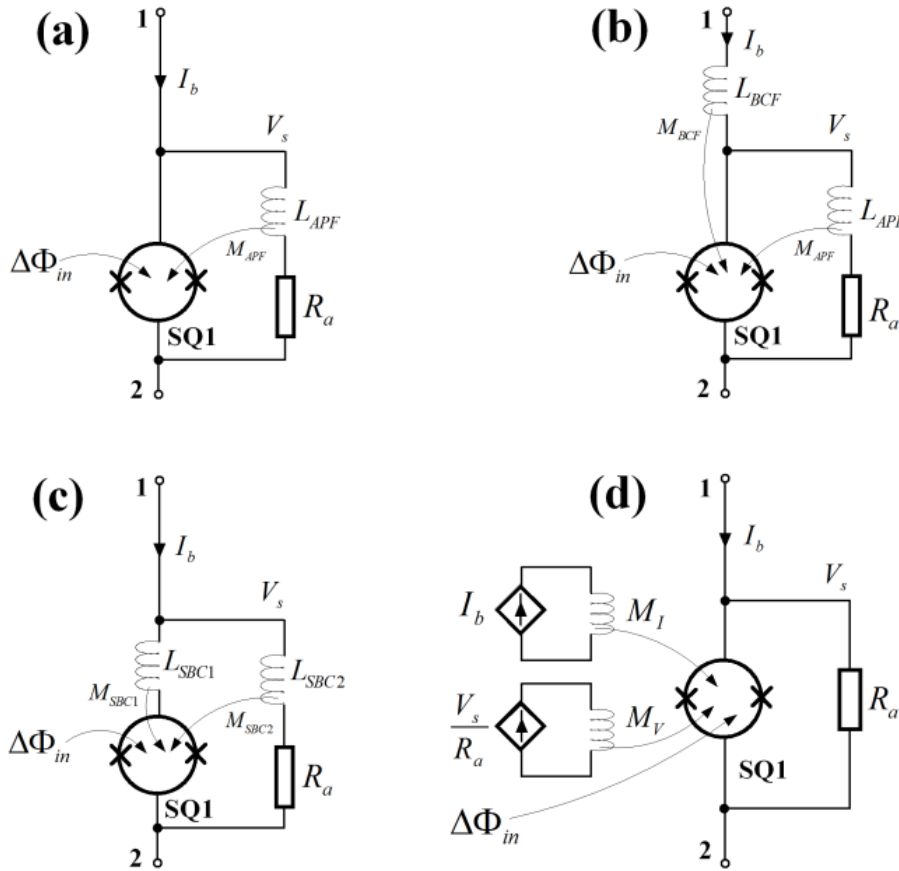


Fig. 4. (a) The APF scheme, (b) The BCF + APF scheme, (c) The SBC scheme, and (d) the general equivalent circuit of internal feedback schemes.

1) The APF scheme is shown in Fig. 4a, in which, SQUID is shunted by a resistor R_a in series with inductance L_{APF} . L_{APF} is coupled to SQ1 with mutual inductance M_{APF} . The flux internally coupled to SQ1 by shunt current through L_{APF} is $M_{APF}V_s / R_a$.

2) Fig. 4b shows the BCF+APF scheme which is the BCF circuit in addition to APF scheme. BCF creates a flux feedback driven by bias current I_b through inductance L_{BCF} , which is coupled to SQ1 with mutual inductance M_{BCF} . The fluxes internally coupled to SQ1 through L_{APF} and L_{BCF} are written as $M_{APF}V_s / R_a - M_{BCF}I_b$. Here, the minus sign indicates the fluxes generated by bias current I_b and shunt current V_s / R_a are opposite.

3) The SBC scheme is also on the basis of APF scheme as shown in Fig. 4c. The inductance used for APF is renamed as L_{SBC2} , and an extra inductance L_{SBC1} is inserted in series with SQ1 which current is $I_b - V_s / R_a$. L_{SBC1} and L_{SBC2} are coupled to SQ1 with mutual inductance M_{SBC1} and M_{SBC2} respectively. If fluxes generated by current through SQ1 and current through R_a are assumed opposite, the total fluxes internally coupled to SQ1 are rewritten as $(M_{SBC1} + M_{SBC2}) V_s / R_a - M_{SBC1} I_b$.

It shows that there are two internal flux feedback modes in those internal feedback schemes. The one driven by I_b is defined as Current Feedback (CFB). The other one driven by V_s is defined as Voltage Feedback (VFB). Their mutual inductances coupled with SQ1 are defined as M_I and M_V . The configurations of M_I and M_V in the schemes shown in Fig. 4 are summarized in Table 1.

Table 1. Configurations of M_V and M_I in different internal feedback schemes.

Scheme	Value of M_V	Value of M_I
APF	$M_V = M_{APF}$	$M_I = 0$
BCF+APF	$M_V = M_{APF}$	$M_I = M_{BCF}$
SBC	$M_V = M_{SBC1} + M_{SBC2}$	$M_I = M_{SBC1}$

Therefore, the internal feedback schemes are equivalent if they are configured with the same M_V and M_I , e.g., the BCF+APF scheme and SBC scheme are equivalent, if $M_{APF} = M_{SBC1} + M_{SBC2}$, and $M_{BCF} = M_{SBC1}$.

All the schemes above are unified with a general equivalent circuit as shown in Fig. 4d. The CFB and VFB circuits are functioned as two flux generators, which one is driven by bias current I_b , and the other one is driven by shunt current V_s/R_a ; they are coupled to SQUID with mutual inductance M_I and M_V respectively. Here, the impedance of inductances is negligible for frequency limit of circuits.

3.2 Small signal analysis of internal feedback circuit

By using SQUID small signal model in the general equivalent circuit, we can have the equivalent small signal circuit of SQUID internal feedback schemes as shown in Fig. 5a.

The current-driven flux generators of CFB and VFB cooperated with small signal SQUID are functioned as two Trans-Impedance Amplifiers (TIAs) [17], which convert current ΔI_b or $\Delta V_s/R_a$ into small voltages. The trans-impedances of TIA are defined with mutual inductances and flux-to-voltage transfer coefficient as:

$$\begin{cases} R_I = \frac{\partial V_s}{\partial \Phi_a} M_I \\ R_V = \frac{\partial V_s}{\partial \Phi_a} M_V \end{cases} \quad (8)$$

With TIA model and concepts of trans-impedances R_I and R_V , circuit in Fig. 5a is internalized into linear circuit as shown in Fig. 5b, in which, SQUID small signal voltage consists of three components, which one is voltage source $(\partial V_s/\partial \Phi_a)\Delta\Phi_{in}$, and the other two are dependant voltage sources $R_I\Delta I_b$ and $R_V\Delta V_s/R_a$.

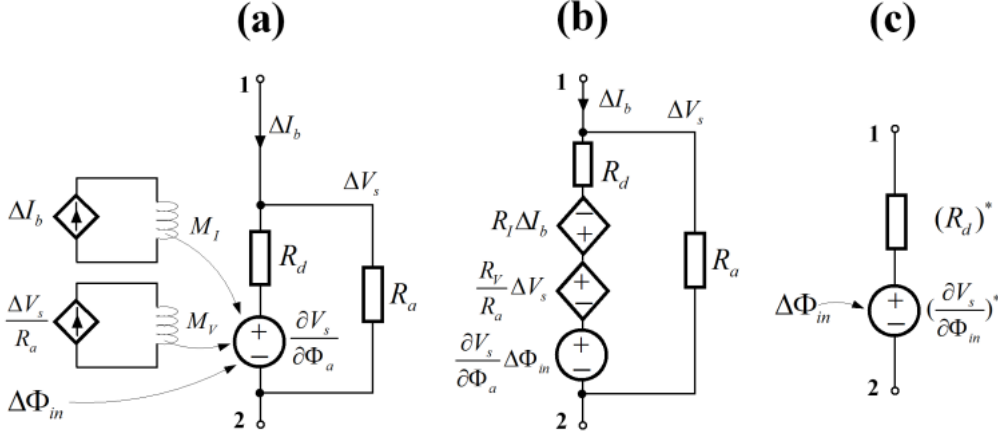


Fig. 5. (a) The equivalent small signal circuit of SQUID internal feedback schemes, (b) The simplified equivalent circuit with TIA model, (c) The unified Thevenin's equivalent circuit of SQUID internal feedback schemes.

Fig. 5c shows the unified Thevenin's equivalent circuit of all the SQUID with internal feedback schemes derived from linear electric circuit in Fig. 5b, where, $(\partial V_s/\partial \Phi_{in})^*$ is the equivalent transfer coefficient and $(R_d)^*$ is the equivalent dynamic resistance, they are written as:

$$\left(\frac{\partial V_s}{\partial \Phi_{in}}\right)^* = \frac{\partial V_s}{\partial \Phi_a} \cdot \frac{1}{1 - (R_V - R_d)/R_a} \quad (9)$$

$$(R_d)^* = R_d \cdot \frac{1 - R_I/R_d}{1 - (R_V - R_d)/R_a} \quad (10)$$

It is shown that the flux-to-voltage transfer coefficient $(\partial V_s/\partial \Phi_{in})^*$ is only improved by VFB with trans-impedance R_V ; while, the dynamic resistance $(R_d)^*$ is increased by VFB with R_V , and decreased by CFB with R_I [12, 13].

The numerators and denominators in (9) and (10) should always be positive to keep circuit stable, thus, the critical conditions of R_I and R_V are derived as:

$$R_I < R_d; R_V < R_d + R_a \quad (11)$$

By using TIA model, SQUID internal feedback schemes are turned into conventional electric circuits, which are easily analyzed with fundamental electric circuit theorems.

4. Low noise direct readout schemes

4.1 Configurations of low noise direct readout schemes

All the low noise direct readout schemes being reported, e.g., APF, NC, BCF+APF, and SBC, are the applications of internal feedback schemes working in CBVA or VBCA mode as shown in Fig. 6. APF and BCF+APF schemes are read out with CBVA, while, NC and SBC schemes are read out with VBCA.

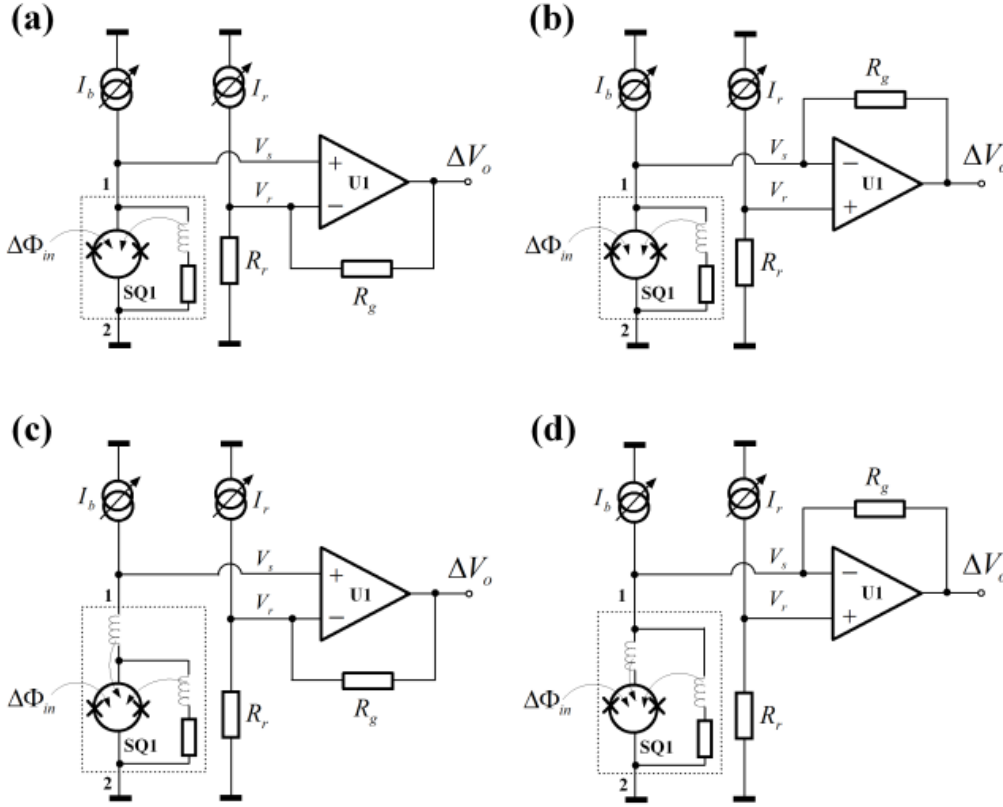


Fig. 6 (a) The APF direct readout circuit, (b) The NC direct readout circuit, (c) The BCF + APF direct readout circuit, and (d) the SBC direct readout circuit.

4.2 Performances improvement

By using the unified Thevenin's equivalent circuit shown in Fig. 5c, we can have the small signal readout circuit of low noise readout schemes as shown Fig. 7a and b. Here, the current noises of preamplifier are neglected if the noise impedance matching condition in (7) is satisfied.

After using internal feedback scheme, the overall amplified transfer coefficients of SQUID direct readout circuits are derived as:

$$\begin{aligned} \left(\frac{\Delta V_o}{\Delta \Phi_{in}}\right)_{CBVA}^* &= \frac{R_g}{R_r} \left(\frac{\partial V_s}{\partial \Phi_{in}}\right)^* \\ &= \left(\frac{\Delta V_o}{\Delta \Phi_{in}}\right)_{CBVA} \frac{1}{1 - (R_V - R_d)/R_a} \end{aligned} \quad (12)$$

$$\begin{aligned}
\left(\frac{\Delta V_o}{\Delta \Phi_{in}}\right)_{VBCA}^* &= -\frac{R_g}{(R_d)^*} \left(\frac{\partial V_s}{\partial \Phi_{in}}\right)^* \\
&= \left(\frac{\Delta V_o}{\Delta \Phi_{in}}\right)_{VBCA} \frac{1}{1-R_I/R_d}
\end{aligned} \tag{13}$$

Compared with the transfer coefficient definitions in (4) and (5), the characteristics read out with CBVA are modified by VFB with trans-impedance R_V , and the characteristics read out with VBCA are modified by CFB with trans-impedance R_I [10, 11].

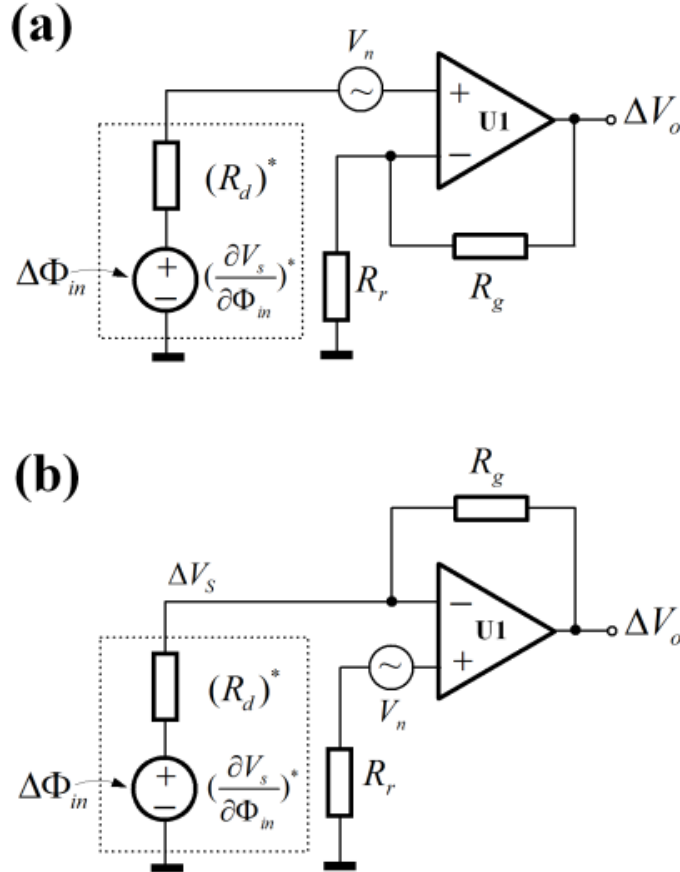


Fig. 7. (a) The small signal equivalent circuit of APF and APF+BCF readout schemes, and (b) the small signal equivalent circuit of NC and SBC readout schemes.

Meanwhile, the equivalent flux noise of amplifier after using internal feedback circuit is rewritten as:

$$\begin{aligned}
(\Phi_n)^* &= \frac{V_n}{(\partial V_s / \partial \Phi_{in})^*} \\
&= \Phi_n \cdot (1 - (R_V - R_d) / R_a)
\end{aligned} \tag{14}$$

Here, Φ_n is the flux noise of preamplifier working with SQUID without internal feedback as defined in (6). Thus, $(1 - (R_V - R_d) / R_a)$ is the noise suppression factor after using internal feedback scheme, and is only decreased by VFB with R_V .

CFB circuit in the readout is only used to regulate dynamic resistance $(R_d)^*$ for noise impedance matching in the applications where current noise is significant [20].

5. Experimental results

The experimental set up for validation of SQUID low noise readout schemes is shown in Fig. 8. The bias and amplifier circuit can be switched between CBVA and VBCA modes by reversing the connections of bias bridge and differential amplifier with a Double-Pole-Double-Throw (DPDT) switch SW1. AD797 (from Analog Device) with white voltage noise of $1\text{nV}/\sqrt{\text{Hz}}$ (at 1k Hz) was used as amplifier directly coupled with SQUID. Its noise impedance R_n is about $500\ \Omega$. Resistor R_p is matching with R_g to balance the input impedances of amplifier, $R_p = R_g$.

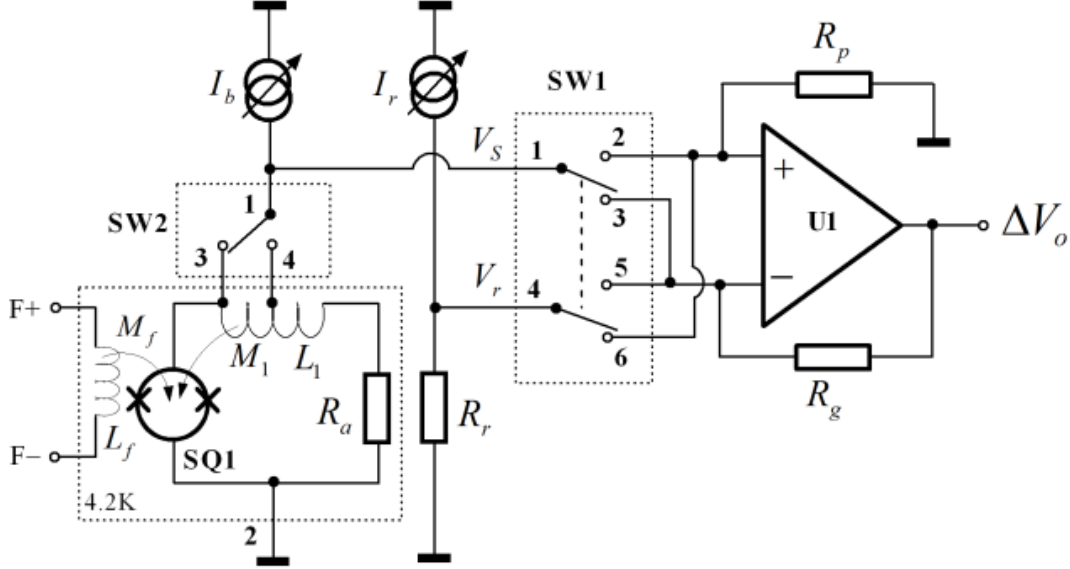


Fig. 8. SQUID direct readout circuit configurable for testing.

Table 2. Parameters of SQUID and readout circuit.

Parameter	Symbol	Value (Unit)
Bias current of SQ1	I_b	$\approx 20\ \mu\text{A}$
Voltage swing of SQ1	$V_{s,pp}$	$\approx 40\ \mu\text{V}$
Loop inductance of SQ1	L_s	$\approx 60\ \text{pH}$
Input coil coupling	$1/M_1$	$\approx 5.8\ \mu\text{A}/\Phi_0$
Feedback coil coupling	$1/M_f$	$\approx 56\ \mu\text{A}/\Phi_0$
Resistor	R_a	$27\ \Omega$
Resistor	R_r	$3\ \Omega$
Resistor	R_g, R_p	$2\ \text{k}\Omega$
FLL feedback resistor	R_f	$10\ \text{k}\Omega$

A low-Tc niobium-based dc SQUID integrated with a feedback coil L_f and an input coil L_1 was applied to build a SQUID internal feedback circuit. A tap was drawn out from L_1 as the third terminal. Two terminals of L_1 were connected to a Single-Pole-Double-Throw (SPDT) switch SW2 (terminal 3 and 4). The mutual inductance of L_1 coupled to SQ1 is M_1 . Mutual inductance of left part between terminal 3 and 4 is kM_1 , where, k is the fraction decided by location of tap; in this

experimental set up, $k \approx 1/6$.

SQUID internal feedback circuit is switched between APF and SBC mode by SW2. When bias current at terminal 1 is connected to terminal 3, the SQ1 is working in APF scheme, where, $M_V = M_1$, $M_I = 0$. It is working in SBC scheme when bias current is connected to terminal 4, where, $M_V = M_1$, $M_I = kM_1$.

The test FLL was set up using an extra integrator and a feedback resistor R_f connected with feedback coil L_f , according to Fig. 1. Parameters of SQUID and readout circuit are shown in Table 2.

The first test case (CASE I) was readout of bare SQUID. SQ1 was working as a bare SQUID in 4.2K liquid helium, where, SW2 was switched to APF mode, and R_a was replaced with a 100 k Ω to avoid input coil resonance. The Φ_{in} -to- V_o characteristics read out with CBVA and VBCA were measured as shown in Fig. 9a and b. and current-voltage characteristics through working point (W_1) was shown in Fig. 9c.

Moreover, an Ultra Low Noise Amplifier (ULNA) which voltage noise is about 0.3nV/ $\sqrt{\text{Hz}}$ [20] was employed in the FLL to make noise performance comparisons with FLLs in CBVA and VBCA modes. The measured noise spectrums are compared in Fig. 9d. In readout of bare SQUID, flux noises measured by FLLs with CBVA and VBCA are about $7.5 \mu\Phi_0 / \sqrt{\text{Hz}}$, while, the flux noise measured with ULNA is reduced to $2 \mu\Phi_0 / \sqrt{\text{Hz}}$.

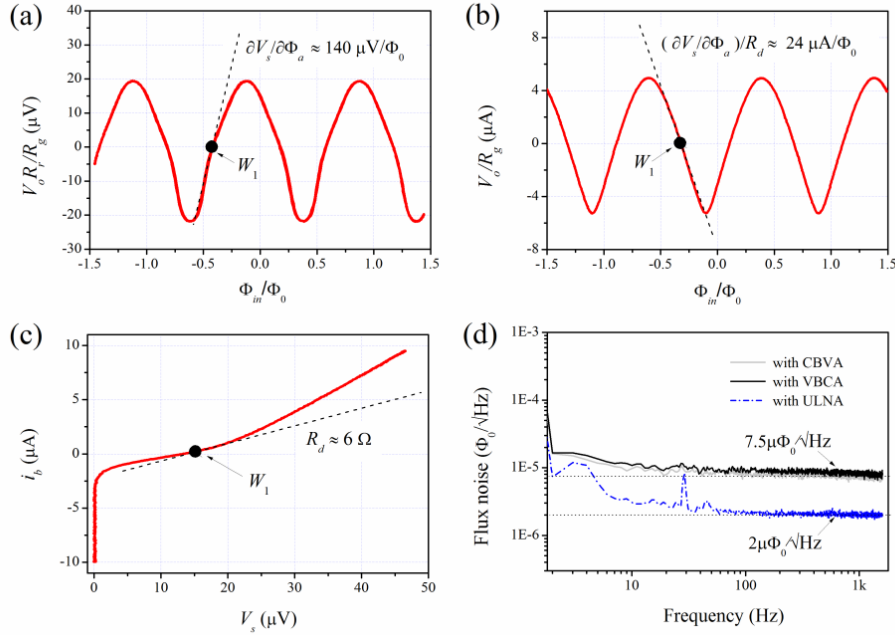


Fig. 9. (a) Φ_{in} -to- V_o characteristics read out with CBVA, (b) Φ_{in} -to- V_o characteristics read out with VBCA, (c) Current-voltage characteristic of SQ1 through the working point, and (d) the noise spectrums of FLL read out with CBVA, VBCA, and ULNA.

The second test case (CASE II) was readout of SQUID in APF mode, where, R_a was set as 27 Ω . The experimental results of overall Φ_{in} -to- V_o characteristics, current-voltage characteristic through working point, and noise spectrums read out

with CBVA and VBCA were shown in Fig. 10.

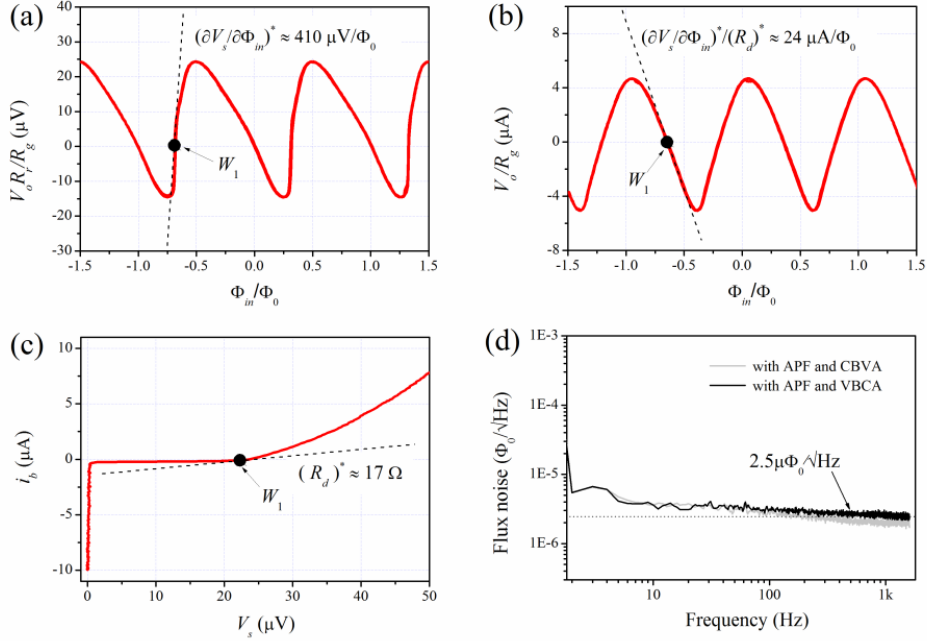


Fig. 10. (a) Φ_{in} -to- V_o characteristics read out with APF and CBVA, (b) Φ_{in} -to- V_o characteristics read out with APF and VBCA, (C) Current-voltage characteristic of SQ1 with APF through working point, and (d) The noise spectrums of FLL read out with APF in both CBVA and VBCA modes.

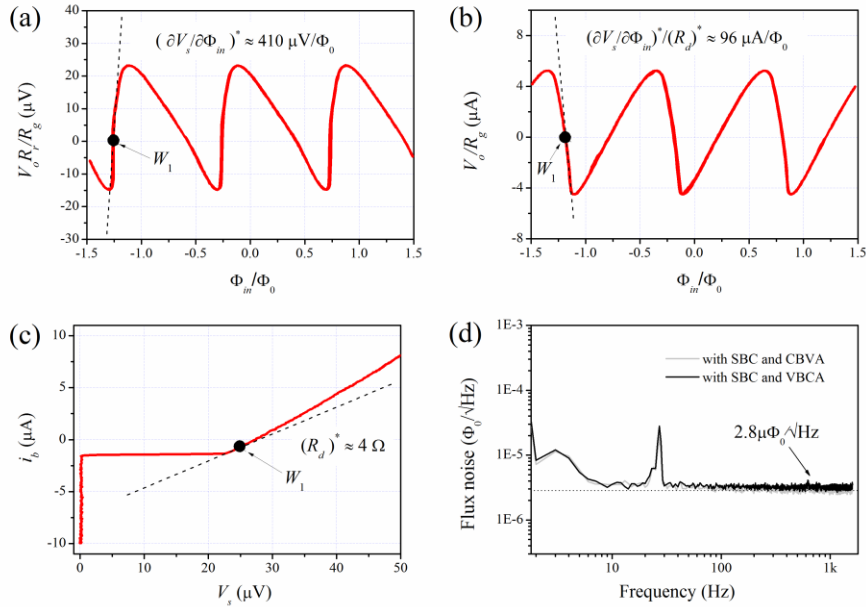


Fig. 11. (a) Φ_{in} -to- V_o characteristics read out with SBC and CBVA, (b) Φ_{in} -to- V_o characteristics read out with SBC and VBCA, (C) Current-voltage characteristic of SQ1 with SBC through working point, and (d) The noise spectrums of FLL read out with SBC in both CBVA and VBCA modes.

The third test case (CASE III) was readout of SQUID in SBC mode switched by SW2, where, R_a was still 27Ω . The experimental results of overall Φ_{in} -to- V_o characteristics, current-voltage characteristic through working point, and noise spectrums read out with CBVA and VBCA were shown in Fig. 11.

From measured Φ_{in} -to- V_o characteristics in three test cases, it is proved that the VFB in APF and SBC schemes turns flux-to-voltage characteristics of SQUID measured with CBVA from symmetrical as shown in Fig. 9a to asymmetrical as shown in Fig. 10a and Fig. 11a. Meanwhile, the CFB in SBC scheme turns flux-to-current characteristics of SQUID measured with VBCA from symmetrical as shown in Fig. 9b to asymmetrical as shown in Fig. 11b.

Four key parameters on the setting working point (W_1) were extracted from all the experimental results as summarized in Table 3.

Table 3. Summary of parameters extracted from experimental results.

Test case	Transfer coefficient measured with CBVA	Value ($\mu\text{V}/\Phi_0$)	Transfer coefficient measured with VBCA	Value ($\mu\text{A}/\Phi_0$)
I	$\partial V_s/\partial\Phi_a$	140	$(\partial V_s/\partial\Phi_a)/R_d$	24
II	$(\partial V_s/\partial\Phi_{in})^*$	410	$(\partial V_s/\partial\Phi_{in})^*/(R_d)^*$	24
III	$(\partial V_s/\partial\Phi_{in})^*$	410	$(\partial V_s/\partial\Phi_{in})^*/(R_d)^*$	96
Test case	Dynamic resistance	Value (Ω)	Equivalent flux noise	Value ($\mu\Phi_0/\sqrt{\text{Hz}}$)
I	R_d	6	Φ_n	7.5
II	$(R_d)^*$	17	Φ_n^*	2.5
III	$(R_d)^*$	4	Φ_n^*	2.8

According to (4) and (12), the flux-to-voltage transfer coefficient $\partial V_s/\partial\Phi_a$ of SQ1 and $(\partial V_s/\partial\Phi_{in})^*$ of SQ1 with APF or SBC circuit were proportional to transfer coefficient of Φ_{in} -to- V_o characteristics read out with CBVA. Meanwhile, the $(\partial V_s/\partial\Phi_a)/R_d$ and $(\partial V_s/\partial\Phi_a)^*/(R_p)^*$ were proportional to transfer coefficient of Φ_{in} -to- V_o characteristics read out with VBCA according to (5) and (13). Dynamic resistance R_d of SQ1 and $(R_d)^*$ of SQ1 with APF and SBC circuit were measured from current-voltage characteristics. Finally, we picked up the equivalent white noise Φ_n with bare SQUID and $(\Phi_n)^*$ with APF and SBC scheme from noise spectrums measured in both VBCA and CBVA modes.

On the setting working point, the $\partial V_s/\partial\Phi_a$ of bare SQ1 is about $140 \mu\text{V}/\Phi_0$, and the dynamic resistance is nearly 6Ω . Therefore, the trans-impedance R_V in both APF and SBC modes is approximately $23\sim 25 \Omega$, and trans-impedance R_I in SBC mode is approximately $4\sim 5 \Omega$, thus, $1/(1-(R_V-R_d)/R_a) \approx 3$, and $1/(1-R_I/R_a) \approx 4$.

In the experimental results, transfer coefficient of SQUID is increased from about $140 \mu\text{V}/\Phi_0$ to $410 \mu\text{V}/\Phi_0$ in both APF and SBC modes; the dynamic resistance is increased from 6Ω to nearly 17Ω in APF mode, and decreased from 17Ω to about 4Ω in SBC mode. Equations (9) and (10) are verified that the flux-to-voltage transfer coefficient is modified only by VFB with R_V , while, the dynamic resistance is increased by VFB and decreased by CFB with R_I .

Meanwhile, flux noise is suppressed from $7.5 \mu\Phi_0/\sqrt{\text{Hz}}$ to $2.5\sim 2.8 \mu\Phi_0/\sqrt{\text{Hz}}$ after

SQUID working in APF and SBC modes with same trans-impedance R_V . However, the flux noise measured with CBVA and VBCA are same in each test case, where, the bias and amplifier configurations have no effect on its noise performance.

In the first test case, the noise performance comparisons between FLL with ULNA and the one with CBVA or VBCA show that, the flux noise Φ_n is directly reduced with the reduction of amplifier noise V_n as described in (6), until it is close to the intrinsic noise of SQUID.

Since, SQUID internal feedback scheme is applied only for noise suppression of preamplifier when amplifier voltage noise V_n dominates the noise performance of the FLL, it will not be necessary if voltage noise of amplifier is below the SQUID intrinsic noise [21].

6. Conclusion

All the existing low noise direct readout schemes such as APF, NC, BCF+APF, and SBC are analyzed according to the configuration of bias mode and internal flux feedback scheme. CBVA and VBCA are two bias and amplifier modes, in which, SQUID is working as a small signal Thevenin's equivalent circuit around the working point. Transfer coefficient $\partial V_s/\partial \Phi_a$ and dynamic resistance R_d of SQUID are the two key parameters deciding the open-loop gain and noise performance of direct readout circuit. They are improved by VFB and CFB circuits in internal feedback schemes.

Analyses and experimental results show that, noise performance is irrelevant to the configurations of bias and amplifier; it is only determined by flux-to-voltage transfer coefficient of SQUID. In the SQUID with internal feedback scheme, transfer coefficient is only improved by VFB with trans-impedance R_V , while, the dynamic resistance is increased by VFB with trans-impedance R_V and decreased by CFB circuit with trans-impedance R_V .

Internal feedback schemes are applied only for noise suppression of amplifier which voltage noise dominates the noise performance of FLL. They will not be necessary if amplifier voltage noise is lower than SQUID intrinsic noise. Thus, finding low cost and lower noise amplifier is the ultimate solution for high performance low noise SQUID direct readout electronics.

Acknowledgements

This work was supported by Shanghai Science and Technology Committee (Grant No: 17511103300).

References

- [1] J. Clarke and A. I. J. I. V. Braginski, New York, "The SQUID Handbook: Fundamentals and Technology of SQUIDS and SQUID Systems Vol. I," p. 27, 2004.
- [2] D. Drung, "High-Tc and low-Tc SQUID electronics," *Superconductor Science and Technology*, vol. 16, no. 12, pp. 1320-1336, 2003.
- [3] R. L. Forgacs and A. Warnick, "Digital - Analog Magnetometer Utilizing Superconducting Sensor," *Review of Scientific Instruments*, vol. 38, no. 2, pp. 214-220, 1967.
- [4] D. Drung, R. Cantor, M. Peters, H. J. Scheer, and H. Koch, "Low - noise high - speed dc

- superconducting quantum interference device magnetometer with simplified feedback electronics," *Applied Physics Letters*, vol. 57, no. 4, pp. 406-408, 1990.
- [5] D. Drung and H. Koch, "An integrated DC SQUID magnetometer with variable additional positive feedback," *Superconductor Science and Technology*, vol. 7, no. 5, pp. 242-245, 1994.
- [6] D. Drung, "Low - frequency noise in low - T_c multiloop magnetometers with additional positive feedback," *Applied Physics Letters*, vol. 67, no. 10, pp. 1474-1476, 1995.
- [7] M. Kiviranta and H. Seppa, "DC-SQUID electronics based on the noise cancellation scheme," *IEEE Transactions on Applied Superconductivity*, vol. 5, no. 2, pp. 2146-2148, 1995.
- [8] H. Seppa, A. Ahonen, J. Knuutila, J. Simola, and V. Volkman, "DC-SQUID electronics based on adaptive positive feedback: experiments," *IEEE Transactions on Magnetics*, vol. 27, no. 2, pp. 2488-2490, 1991.
- [9] D. Drung, "Recent low temperature SQUID developments," *IEEE Transactions on Applied Superconductivity*, vol. 4, no. 3, pp. 121-127, 1994.
- [10] M. Kiviranta, "SQUID linearization by current-sampling feedback," *Superconductor Science and Technology*, vol. 21, no. 4, 2008.
- [11] X. Xie *et al.*, "A voltage biased superconducting quantum interference device bootstrap circuit," *Superconductor Science and Technology*, vol. 23, no. 6, 2010.
- [12] Y. Wang *et al.*, "Voltage Biased SQUID Bootstrap Circuit: Circuit Model and Numerical Simulation," *IEEE Transactions on Applied Superconductivity*, vol. 21, no. 3, pp. 354-357, 2011.
- [13] D. Drung, "Simplified analysis of direct SQUID readout schemes," *Superconductor Science and Technology*, vol. 23, no. 6, 2010.
- [14] M. Gershenson, "Performance analysis of modified flux-locked-loop additional positive feedback SQUID," *IEEE Transactions on Applied Superconductivity*, vol. 7, no. 1, pp. 23-26, 1997.
- [15] J. Zeng *et al.*, "Analysis of a dc SQUID readout scheme with voltage feedback circuit and low-noise preamplifier," *Superconductor Science and Technology*, vol. 27, no. 8, 2014.
- [16] H. Weinstock, *SQUID sensors: fundamentals, fabrication and applications*. Springer Science & Business Media, 2012.
- [17] S. Franco, *Design with operational amplifiers and analog integrated circuits*. McGraw-Hill New York, 2002.
- [18] C. K. Alexander, M. N. Sadiku, and M. Sadiku, *Fundamentals of electric circuits*. McGraw-Hill New York, 2009.
- [19] J. Zeng *et al.*, "Study of weakly damped superconducting quantum interference devices operated in different bias modes in presence of external shunt resistance," *Applied Physics Letters*, vol. 103, no. 12, 2013.
- [20] G. Zhang, Y. Zhang, T. Hong, H. Wang, H.-J. Krause, and X. Xie, "Practical dc SQUID system: Devices and electronics," *Physica C: Superconductivity and its Applications*, vol. 518, pp. 73-76, 2015.
- [21] S. A. Gudoshnikov *et al.*, "Direct-coupled electronics for high-temperature superconductor DC SQUID-based magnetometer," *IEEE Transactions on Instrumentation and Measurement*, vol. 46, no. 2, pp. 624-628, 1997.